LETTERS
PUBLISHED ONLINE: 9 FEBRUARY 2015 | DOI: 10.1038/NPHOTON.2015.6
nature photonics

Single-junction polymer solar cells with high efficiency and photovoltage

Zhicai He[1], Biao Xiao[1], Feng Liu[2], Hongbin Wu[1]*, Yali Yang[3], Steven Xiao[3], Cheng Wang[4], Thomas P. Russell[2] and Yong Cao[1]

Polymer solar cells are an exciting class of next-generation photovoltaics, because they hold promise for the realization of mechanically flexible, lightweight, large-area devices that can be fabricated by room-temperature solution processing[1,2]. High power conversion efficiencies of ~10% have already been reported in tandem polymer solar cells[3]. Here, we report that similar efficiencies are achievable in single-junction devices by reducing the tail state density below the conduction band of the electron acceptor in a high-performance photoactive layer made from a newly developed semiconducting polymer with a deepened valence energy level. Control over band tailing is realized through changes in the composition of the active layer and the structure order of the blend, both of which are known to be important factors in cell operation[4–6]. The approach yields cells with high power conversion efficiencies (~9.94% certified) and enhanced photovoltage.

To date, the best reported power conversion efficiency (PCE) of state-of-the-art single-junction polymer solar cells (PSCs) is ~9–10%[7–9], which still lags behind those of the most efficient tandem cells, mainly due to the relatively small absorption overlap with the solar spectrum. To overcome this limitation, the most straightforward strategy is to use narrow-bandgap ($E_g < 1.6$ eV) polymers for light harvesting[2,10,11]. However, a proof of concept of PSCs based on state-of-the-art narrow-bandgap polymers found efficiencies below 9%, despite the fact that the internal quantum efficiency of these materials systems can reach 100%. This implies that the efficiency of PSCs based on these narrow-bandgap polymers is mainly limited by the low open-circuit voltage (V_{OC}), as this was found to correlate directly with the bandgap of the blend, that is, the difference between the lowest unoccupied molecular orbital (LUMO) of the acceptor and the highest occupied molecular orbital (HOMO) of the donor[12,13]. Furthermore, large energy loss during the dissociation of tightly bound photo-induced electron–hole pairs and the generation of free charge carriers will lead to an additional reduction in V_{OC}, which can be described empirically[12,13]. Many other factors, such as the formation of ground-state charge-transfer states between polymer and fullerene[14], varying donor/acceptor fraction[15–17], charge recombination kinetics and charge lifetime (showing an apparent dependence on illumination intensity and temperature)[18–22], have been identified as important factors affecting V_{OC}. Thanks to the use of some powerful characterization techniques such as impedance spectroscopy[19], charge extraction[22] and transient photovoltage[20–22], research in the past few years has significantly increased our knowledge about charge kinetics in operating devices. In addition, recent studies have also confirmed that the density of states (DOS) for the LUMO of the acceptor and the HOMO of the donor and their energetic disorder[4–6] could have significant functional importance in determining V_{OC}.

Here, we demonstrate that fundamental losses in the open-circuit voltage of PSCs based on narrow-bandgap polymers can be effectively alleviated and modulated over a wide range (100 mV) through control over band tailing below the LUMO of $PC_{71}BM$, and we report a PCE of over 10% in single-junction PSCs. By combining the results of analysis of the electrical photocurrent spectral response characteristics of working devices and the results from structural characterizations, we identify that a reduction in band tailing and a concomitant increase in the splitting of the electron and hole quasi-Fermi levels are responsible for the improved open-circuit voltage. Furthermore, we established a correlation between the band tailing and the photovoltage output of the device, and thus can provide more insight into the origins of the high V_{OC}, providing guidelines for further improvement.

To improve the PCE of PSCs toward 10%, one viable strategy is to use a narrow-bandgap polymer that can deliver both a relatively high open-circuit voltage and a high current density, as the donor material. Accordingly, the PSCs here were fabricated from a blend of [6,6]-phenyl C_{71}-butyric acid methyl ester ($PC_{71}BM$) and a newly synthesized narrow-bandgap semiconducting polymer poly [[2,6′-4,8-di(5-ethylhexylthienyl)benzo[1,2-*b*;3,3-*b*] dithiophene] [3-fluoro-2[(2-ethylhexyl)carbonyl]thieno[3,4-*b*]thiophenediyl]] (PTB7-Th), which was prepared as described in the Supplementary Information. A similar polymer was recently reported by Liao and colleagues, who obtained a PCE of 9.4%[7]. When compared with the promising narrow-bandgap semiconducting polymer thieno [3,4-*b*]thiophene/benzodithiophene (PTB7)[10], which can delivery a high PCE of ~9%[7], the electron-donor polymer PTB7-Th has an even narrower bandgap (1.59 eV, with an absorption onset at ~780 nm, Fig. 1a), which is closer to the optimum bandgap (~1.1–1.5 eV) for a single-junction cell, as proven by Shockley and Queisser after considering all optical losses[13]. Figure 1a shows the spectral dependence of the absorption coefficient for a set of films with different PTB7-Th:$PC_{71}BM$ blend ratios, as well as the photon flux of the AM 1.5G solar spectrum for comparison. It is clear that the blends show strong absorption in the region between 500 and 800 nm (where the solar photon flux is maximum), which is a prerequisite for efficient solar energy conversion. Furthermore, PTB7-Th has a HOMO of −5.22 eV (~0.07 eV deeper than that of PTB7)[7], which is also very close to the ideal energy levels[13]. It is therefore expected that the PTB7-Th devices can simultaneously deliver higher V_{OC} and short-circuit current density (J_{sc}) than the PTB7 devices[12,13].

The validity of the fluorine substituent method for a deepened HOMO level and PTB7-Th as a promising electron donor can be

[1]Institute of Polymer Optoelectronic Materials and Devices, State Key Laboratory of Luminescent Materials and Devices, South China University of Technology, Guangzhou 510640, China. [2]Department of Polymer Science and Engineering, University of Massachusetts, Amherst, Massachusetts 01003, USA. [3]1-material Inc., 2290 St-Francois, Dorval, Quebec H9P 1K2, Canada. [4]Advanced Light Source, Lawrence Berkeley National Laboratory, Berkeley, California 94720, USA. *e-mail: hbwu@scut.edu.cn

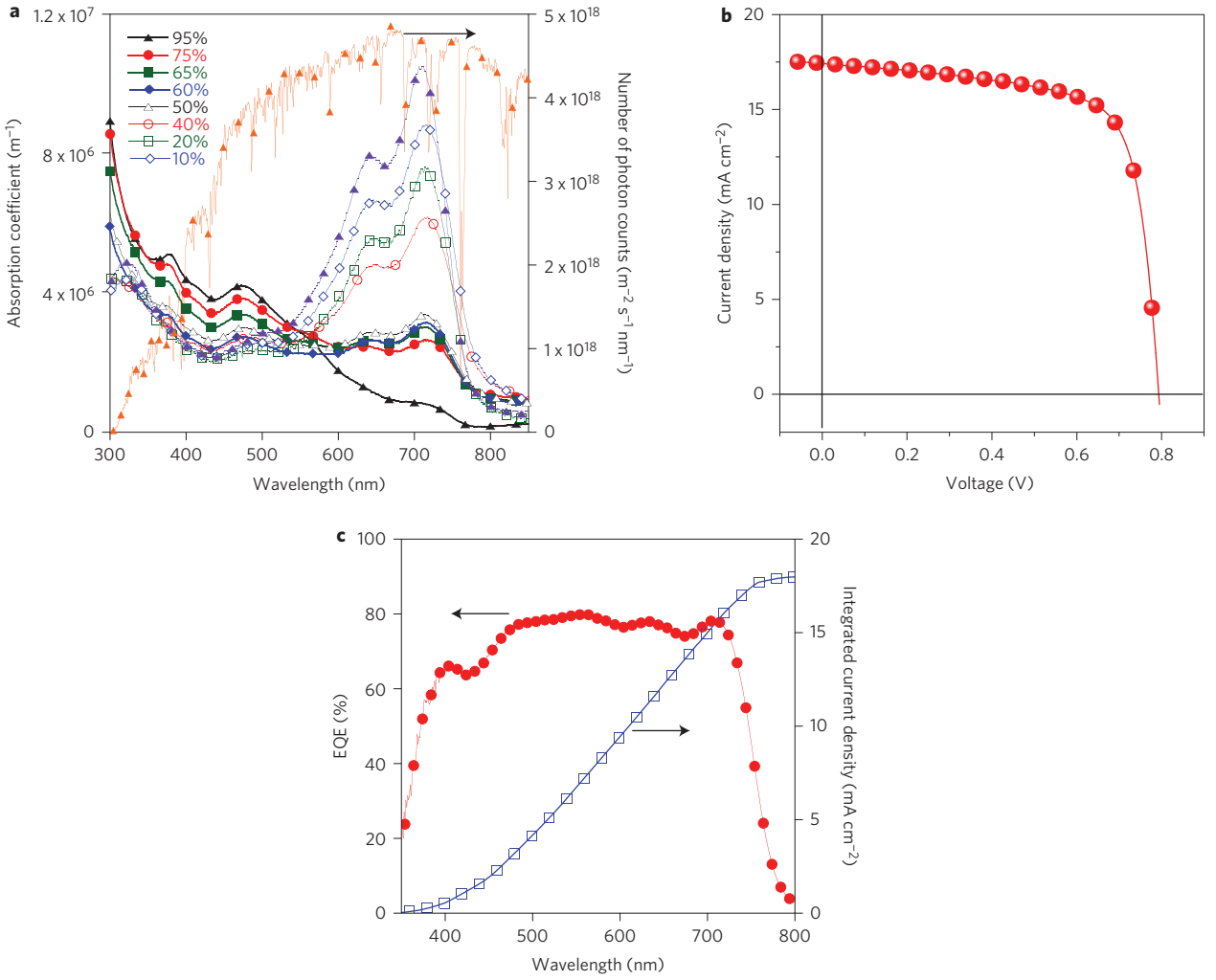

Figure 1 | Optical properties of the blends and device performance of PSCs with 60 wt% $PC_{71}BM$. a, Absorption coefficients of pristine spectra of PTB7-Th and PTB7-Th:$PC_{71}BM$ blends in various ratios. Open diamonds, squares, circles and triangles: blend films with 10, 20, 40 and 50 wt% $PC_{71}BM$, respectively. Filled diamonds, squares, circles and triangles: blend films with 60, 65, 75 and 95 wt% $PC_{71}BM$, respectively. Purple filled triangles: pure polymer film. For comparison, the photon flux of the AM 1.5G solar spectrum is shown on the right axis. **b**, *J*–*V* characteristics of the best performing PSCs with 60 wt% $PC_{71}BM$ in the active layer (certificated at CPVT). **c**, External quantum efficiency (EQE)/incident photon to current efficiency (IPCE) spectra of the corresponding best-performing PSCs (red circles). The integrated product of the IPCE spectrum with AM 1.5G photon flux is also shown (blue squares).

confirmed by the photovoltaics properties and photoresponse of the devices. We first investigated the performance of devices in an inverted structure[7] with a regular composition in which the polymer:$PC_{71}BM$ ratio was 1:1.5. Characterization of the PSCs under 1 sun, 1,000 W m^{-2}, AM 1.5G illumination in ambient air at our home laboratory demonstrated very good device performance. Device parameters such as V_{OC}, J_{sc} and fill factor (FF) deduced from the *J*–*V* characteristics of the most efficient devices were 0.815 V, 17.52 mA cm^{-2} and 72.0% (Table 1), respectively, yielding a high efficiency of 10.28%. When compared with the performance of the best PTB7 devices in our previous report (V_{OC} = 0.740 V, J_{sc} = 17.20 mA cm^{-2}, FF = 72.0% and PCE = 9.15%[7]), the PTB7-Th devices have both higher V_{OC} and higher J_{sc}, indicating that the fluorine substituent method is indeed a very successful strategy for increasing V_{OC} by deepening the LUMO levels and enhancing the photocurrent by lowering the bandgap of the polymer.

After encapsulation, a series of devices with an initial PCE of ~10.3% were sent to the National Center of Supervision & Inspection on Solar Photovoltaic Products Quality of China (CPVT) for certification. A certified PCE of 9.939% was achieved (Fig. 1b and Supplementary Fig. 1), with a V_{OC} of 0.7936 V, J_{sc} of 17.42 mA cm^{-2} and fill factor of 71.9%. To the best of our knowledge, this is a new record high efficiency for a single-junction PSCs.

Figure 1c presents the external quantum efficiency (EQE) of the devices, showing the spectral response spanning from the ultraviolet to the near-infrared (NIR) (350 nm to 800 nm). A peak EQE of 80% at 550 nm is clearly seen, and an average EQE of 74% in

Table 1 | Best device performance/parameters from PTB7-Th devices with different $PC_{71}BM$ weight fractions in the active layer, measured under 1,000 W m^{-2} AM 1.5G illumination.

$PC_{71}BM$ (%)	V_{OC} (V)	J_{sc} (mA cm^{-2})	FF (%)	PCE (%)
10	0.720	3.31	44.05	1.04
20	0.801	6.84	38.88	2.13
40	0.804	16.61	68.11	9.09
50	0.806	17.18	66.15	9.16
60	0.815	17.52	72.01	10.28
65	0.825	17.43	73.78	10.61
75	0.832	15.82	69.01	9.08
95	0.840	7.31	69.53	4.27

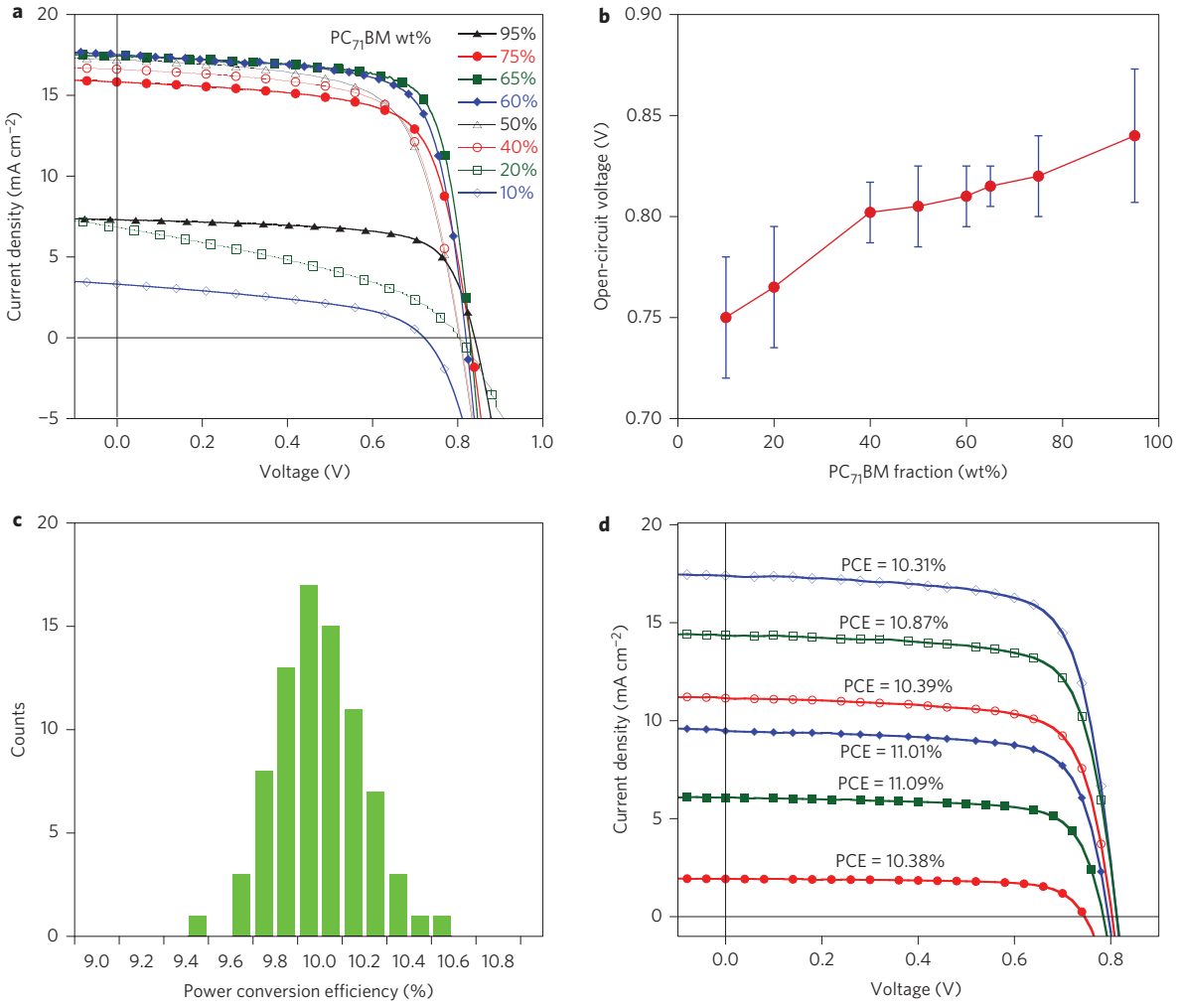

Figure 2 | Tunable photovoltage output control and photocurrent density–voltage characteristics of a device with 65 wt% $PC_{71}BM$ under simulated AM 1.5G sunlight with different illumination intensities. a, Typical *J*–*V* characteristics of PTB7-Th devices with different $PC_{71}BM$ weight fractions in the active layer. With an increase in $PC_{71}BM$ content the shift in V_{OC} was found to be 115 mV. **b**, Device parameter V_{OC} deduced from *J*–*V* measurements. Experimental error bars represent one standard deviation from a set of ten experimental measurements for each type of device. **c**, Histogram of PCE counts for 80 individual devices with 65 wt% $PC_{71}BM$ in the active layer. **d**, *J*–*V* characteristics of a device with 65 wt% $PC_{71}BM$ in the active layer tested under different illumination conditions, as obtained from standard AM 1.5G (1,000 W m^{-2}) illumination using a set of neutral optical filters.

nearly the entire visible region (~400–750 nm). Note that the theoretical J_{sc} obtained by integrating the product of the EQE data and the AM 1.5G solar spectrum is 17.99 mA cm^{-2}, which is in good agreement with the values obtained from the *J*–*V* characteristics (Fig. 1b, Table 1).

To further enhance the V_{OC} and overall device performance in the PTB7-Th devices we identified that a key design parameter—the composition—can have a big impact on the device characteristics. The extracted best device performances for devices with varying $PC_{71}BM$ weight fractions in a wide range between 10 and 95% are summarized in Table 1, and the typical corresponding *J*–*V* characteristics are plotted as a series of curves in Fig. 2a. Experimentally, the measured V_{OC} showed a monotonic increase as the $PC_{71}BM$ weight fraction increased, as shown in Fig. 2b, in which statistics analyses are included. For example, in the low $PC_{71}BM$ weight fraction regime the device demonstrated average V_{OC} values of 0.750 V (10 wt%) and 0.764 V (20 wt%), increasing to 0.820 V (75 wt%) and 0.841 V (95 wt%) in the high $PC_{71}BM$ loading regime, but at the expense of decreasing J_{sc}. We also note that the FF also showed a nearly monotonic increase from 43 to 73% as the $PC_{71}BM$ weight fraction increased from 10 to 65 wt%, mainly due to improved electron mobility[13]. In the higher $PC_{71}BM$ loading regime (75 and 95 wt%), the FF remained as high as 67–69%, indicating very efficient exciton dissociation and charge separation efficiency in the devices[13].

The observed trend is consistent with earlier results in other systems[16,17], but is in direct contrast with previous observations by Janssen and colleagues[15] and Garcia-Belmonte and co-workers[23], respectively. As revealed in ref. 15, charge transfer states are the crucial intermediate step between exciton dissociation and charge separation, the efficiencies of which are strongly dependent on the aggregation of PCBM. On the other hand, because our devices displayed high FF for a wide range of PCBM contents, we conclude that exciton dissociation and charge generation are not the major limiting factors in our devices, and the central findings by Janssen and colleagues[15] may not be completely applicable to this study. We also note that in the case of the existence of charge transfer between the PCBM and the metal electrode and the concomitant formation of an interfacial dipole, an opposite trend in V_{OC} versus PCBM was found[23]. However, this can be excluded in this study because significant charge transfer would not take place as the indium tin oxide (ITO)/poly[(9,9-bis(3′-(*N*,*N*-dimethylamino)

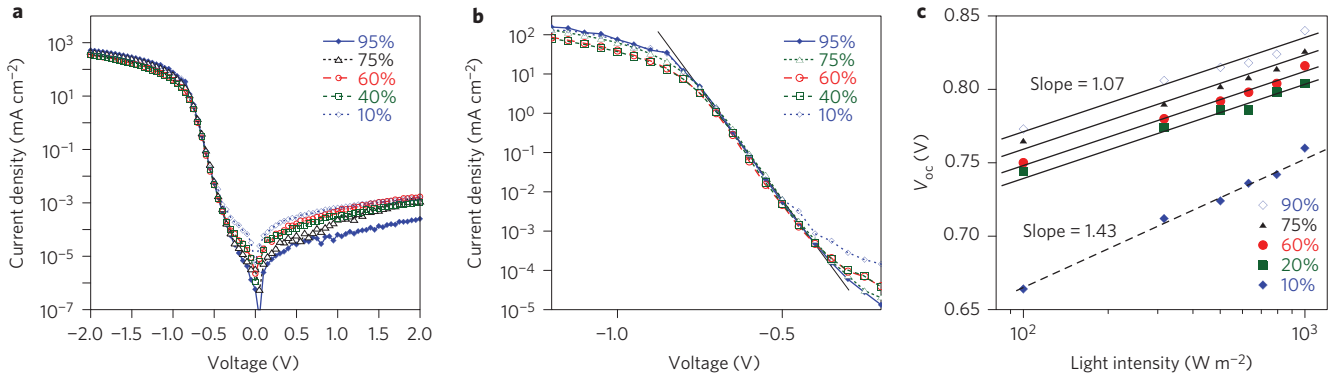

Figure 3 | Dark *J*–*V* characteristics of devices and dependence of V_{OC} on light intensity *I*. **a**, Dark *J*–*V* characteristics of a series of typical devices with different $PC_{71}BM$ contents. **b**, Reproduction of the data in **a**. The solid black line corresponds to a best fit to the exponential increase in dark *J*–*V* characteristics. **c**, V_{OC} versus natural logarithm of light intensity ($V_{OC} \sim \ln I$) for the devices. Black solid lines represent the best fitting results with a slope of 1.07, and the black dashed line corresponds to a slope of 1.43. Within the margins of experimental error, the dependence of V_{OC} on *I* is essentially identical for all devices with a $PC_{71}BM$ content of more than 20%, following $dV_{OC} = (1.10 \pm 0.10)(q/kT)d \ln I$, suggesting that bimolecular recombination is the dominant loss mechanism. A $PC_{71}BM$ content (10 wt%) that is too low will lead to a deviation.

propyl)-2,7-fluorene)-*alt*-2,7-(9,9–dioctylfluorene)] (PFN) formed an ohmic contact with the PCBM[7].

As a result of a balance compromise between absorption, photovoltage output and charge transport/collection, devices based on a relatively higher $PC_{71}BM$ loading (that is, 65 wt%) deliver even better device performance. To demonstrate the reproducibility of the results, 80 individual devices were fabricated under this optimized condition, and the histogram of the test results is shown in Fig. 2c. Indeed, the results show very good reproducibility, with an average PCE of 10.09% and a standard deviation of 0.20%. Among these devices, the best showed a PCE of 10.61%, with a V_{OC} of 0.825 V, J_{sc} of 17.43 mA cm^{-2} and fill factor of 73.78%. This high PCE reported here is one of the best results for single-junction PSCs[9], and is also comparable with those of the best amorphous/microcrystalline Si solar cells (~10.1%/10.7%)[13] or organic tandem cells (~10.6%)[3].

Furthermore, our devices show excellent device performance at relatively low light intensity conditions. Figure 2d shows the *J*–*V* characteristics of a typical device under different incident illumination conditions (all performance parameters are summarized in Supplementary Table 1 for comparison). It can be seen that the devices show a PCE of 10.31% under standard AM 1.5G illumination, and this value improves to 11.01 and 11.09% at lower light intensities of 501 and 316 W m^{-2} (obtained by a set of neutral optical filters), respectively. A further decrease in light intensity will lead to a drop in PCE (~10.38%) due to the decrease in V_{OC}. Other devices show a similar trend following a change in illumination intensity (Supplementary Fig. 2, Supplementary Table 1). Nevertheless, in contrast to inorganic solar cells, which are typically more efficient when exposed to high illumination intensities (through a solar concentrator), PSCs can be more efficient (than their nominal efficiency) under low-intensity illumination (most often encountered outdoors or indoors). This advantage potentially makes organic/polymer photovoltaics suitable for large-area applications where a solar concentrator is usually absent.

To investigate the mechanism responsible for V_{OC} enhancement, we first analysed the dark saturation current J_0 of the devices, which can be considered a direct and unambiguous measurement of recombination loss in solar cells, where recombination loss is a fundamental process determining V_{OC} (refs 18, 20). Figure 3a presents the dark *J*–*V* characteristics of a series of typical devices with different $PC_{71}BM$ weight fractions in the active layer. Notably, to a first approximation, all the dark *J*–*V* characteristics show very similar trends, suggesting that the difference in dark saturation current is negligible. A more precise determination of J_0 and other related parameters using the Shockley equation is shown in Supplementary Fig. 3 and Supplementary Table 2, and also confirms this observation. Accordingly, the minor variation in J_0 (less than one order of magnitude) between the devices in fact only corresponds to a shift of a few tens of millivolts or less in V_{OC}. Therefore, the observed increase in V_{OC} should not be ascribed to a reduced recombination rate and the concomitant suppressed dark saturation current.

Further proof of the weak dependence of recombination on $PC_{71}BM$ content comes from the measurement for the ideality factor of the devices in the dark and under illumination, which is a valuable indicator for the type of recombination[24]. Surprisingly, as can be observed from Fig. 3a,b, all the curves show nearly identical slope in the exponential increase regime, resulting in an identical ideality factor value of 1.45 ± 0.15 for all sets of data. In parallel, the ideality factors of the devices under illumination are found to be 1.10 ± 0.10 for most devices, as determined from the slope of V_{OC} versus the natural logarithm of light intensity ($V_{OC} \sim \ln I$; Fig. 3c). Thus, the charge dynamics do not vary significantly between the devices. Indeed, from this observation, we can rule out reduced recombination loss as the origin of the improved V_{OC} in this series of devices.

Only considering differences in charge recombination loss is insufficient to explain the observed enhancement in V_{OC} in the devices. The findings of the present study are consistent with recent suggestions by Garcia-Belmonte and Bisquert and colleagues that reduced energy disorder and the concomitant reduction in band tailing in the donor/acceptor material domain can effectively increase the splitting of the electron and hole quasi-Fermi levels at a given carrier density, resulting in an enlarged, achievable open-circuit voltage in PSCs[5,6,25,26]. To provide strong evidence that the high photovoltage output is truly linked with the reduction in tail state density, we further probed the DOS by photocurrent spectral response measurements, following well-established literature procedures[27]. As shown in Fig. 4a, noticeable photocurrent responses were clearly observed in the region below the optical bandgap of the polymer (1.6 eV) for all devices. The response of all devices showed a clear dependence on photon energy, which can be explained by considering the existence of Gaussian DOSs in the band tails[4–6,25,28]. Furthermore, DOSs were reduced significantly following an increase in $PC_{71}BM$ content, mainly due to increased aggregation in PCBM, as described in the following.

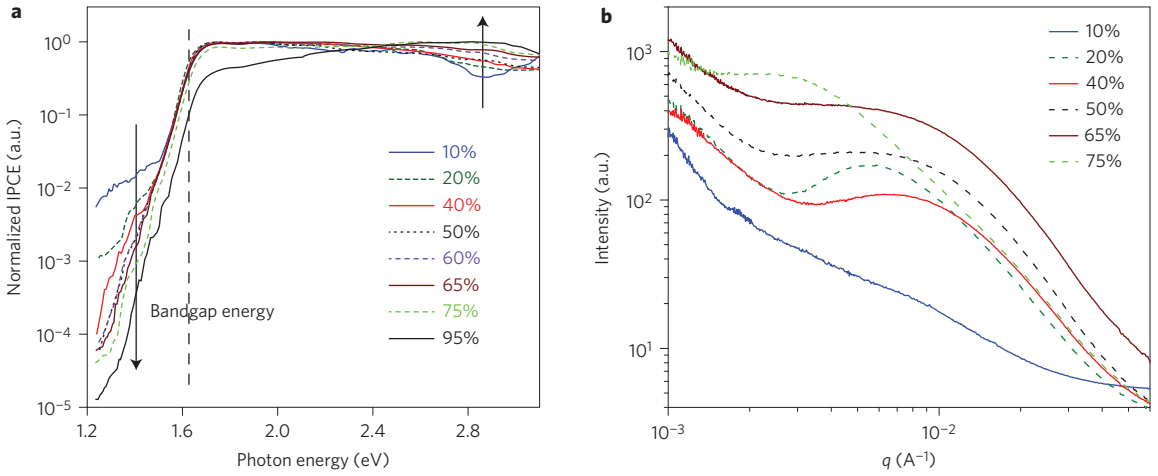

Figure 4 | Photocurrent spectral response characteristics of working devices and structure characterization of the photoactive films. a, UV-vis-NIR spectral responses of devices with different $PC_{71}BM$ weight fractions in the active layer. **b**, Resonant soft X-ray scattering of PTB7-Th:$PC_{71}BM$ blends with different $PC_{71}BM$ contents.

Figure 4b shows the size scale of phase separation using resonant soft X-ray scattering (RSoXS). At a low 10% $PC_{71}BM$ loading, no obvious phase separation is seen due to the good miscibility of the polymer and $PC_{71}BM$[29]. On increasing this content to 20%, a scattering peak at $q = 0.0056$ Å^{-1} (corresponding to a length scale of 112 nm, where q is the scattering vector) maps the phase separation of the conjugated polymer and polymer:$PC_{71}BM$ mixing region. In both cases, the $PC_{71}BM$ cannot form a pure aggregated domain, leading to band tails that are not optimized for a good V_{OC}. When $PC_{71}BM$ loading was increased from 40 to 65%, a similar characteristic length scale (~0.0013 Å^{-1}, corresponding to a length scale of 48 nm) in phase separation is seen, suggesting the same phase structure. The enhanced scattering intensities from 40 to 65% indicate a domain purity improvement[30], and therefore better $PC_{71}BM$ aggregated domain forms. Enhanced aggregation of $PC_{71}BM$, or higher phase purity, reduces the tail state in DOSs, leading to a further enhancement in V_{OC}. Further increasing the $PC_{71}BM$ content (75%) leads to a larger phase separation (~0.0035 Å^{-1}, corresponding to a length scale of 179 nm), yielding a reduction in J_{sc} but still a high V_{OC}, because the $PC_{71}BM$ domain is still well aggregated. More characterizations on morphology are summarized in Supplementary Figs 4–6. We have now established a correlation between the reduction in band tailing and a concomitant increase in photovoltage output of the devices and increased aggregation in PCBM.

In conclusion, we have demonstrated highly efficient single-junction PSCs with PCEs exceeding 10%, representing an important step towards the realization of economical solar cells with a high efficiency that is comparable with those of the best amorphous/microcrystalline Si solar cells or the best organic tandem cells reported to date. Our devices show an excellent PCE of 11% at relatively low light intensity conditions (0.3–0.5 sun illumination). This is achieved by using a newly synthesized narrow-bandgap semiconducting polymer with deep HOMO levels in conjunction with control of the tail state density below the conduction band of the electron acceptor and the disorder degree of the blend. As a result, the fundamental losses in the open-circuit voltage of PSCs based on narrow-bandgap polymers can be effectively alleviated and modulated over a wide range of 100 mV. It should be noted that this strategy to modulate V_{OC} is also applicable to many other typical donor materials. When compared with perovskite solar cells, it is clear that the major lag behind in PSCs is V_{OC}. We therefore argue that PSCs can be as efficient as perovskite solar cells if the V_{OC} in devices based on a narrow-bandgap polymer can be enhanced to 1 V without significant loss in J_{sc}. It will therefore be of interest in the near future to fully exploit the potential of emerging new polymer electron donors by using a high load of $PC_{71}BM$ in the blend. These findings should lead to great advances in other polymer donor materials with a view to achieving even higher efficiency.

Methods

Fabrication of PSCs. Electron acceptor $PC_{71}BM$ was purchased from Aldrich and used as received. Cathode interface material poly[(9,9-bis(3′-(*N*,*N*-dimethylamino) propyl)-2,7-fluorene)-*alt*-2,7-(9,9–dioctylfluorene)] (PFN) was provided by 1-material Inc. and used as received. The poly(3,4-ethylenedioxythiopene):poly (styrenesulphonate) (PEDOT:PSS, Clevios P AI4083) was obtained from H.C. Starck Clevios GmbH. The inverted device structure was ITO/PFN/PTB7-Th:$PC_{71}BM$ (x wt%, where x varied from 10 to 95)/MoO_3/Al, as described in a previous report[7]. Before deposition of the photoactive layer, a PFN thin layer was coated on top of the precleaned ITO substrate (treated by oxygen plasma cleaning for 4 min) by spin-casting from a methanol solution at 2,000 r.p.m. for 1 min, forming a thin interlayer with an initial thickness of 10 nm. The thickness of the interlayer was determined by a surface profiler (Alfa Step-500, Tencor), in conjunction with extrapolation from an absorbance–thickness curve that assumes a linear dependence of absorbance at 380 nm on film thickness. The PFN solution was prepared by dissolving the solid in methanol (anhydrous grade, 99.8%) in the presence of a small amount of acetic acid (~2–20 μl ml^{-1}, depending on the molecular weight of the PFN). The typical concentration of PFN solution for spin-coating is 2 mg ml^{-1}. Following deposition of the PFN interlayer, the PTB7-Th:$PC_{71}BM$ active blend layer, with a nominal thickness of ~80–100 nm, was prepared by spin-coating a mixed solvent of chlorobenzene/1,8-diiodoctane (97%:3% by volume) solution (with a total concentration of 25 mg ml^{-1}) at 1,000 r.p.m. for 2 min. The resulting photoactive layer was dried in vacuum for 3 h before electrode deposition. A 10 nm MoO_3 layer and a 100 nm Al layer were subsequently evaporated through a shadow mask to define the active area of the devices (~2 × 8 mm^2) and form the top anode.

Characterization and measurements[7]. The PCE was determined from *J*–*V* curve measurements (using a Keithley 2,400 sourcemeter) under a 1 sun, AM 1.5G spectrum from a solar simulator (Oriel model 91,192; 1,000 W m^{-2}). Masks made using laser beam cutting technology to have a well-defined area of 3.14 or 16.0 mm^2 were attached to define the effective area for accurate measurement. All the masked and unmasked tests gave consistent results with relative errors within 5%. The solar simulator illumination intensity was determined using a monocrystal silicon reference cell (Hamamatsu S1133, with KG-5 visible colour filter) calibrated by the National Renewable Energy Laboratory (NREL). Theoretical J_{sc} values obtained by integrating the product of the EQE with the AM 1.5G solar spectrum agreed with the measured value to within 3%. PCE statistics were obtained using 80 individual devices fabricated under the same conditions. The varying incident light intensity was obtained from AM 1.5G illumination using a set of neutral optical filters with optical densities of 0.1, 0.2, 0.3, 0.5 and 1, resulting in a series of light intensities of 794, 631, 501, 316 and 100 W m^{-2}, respectively. The UV-vis-NIR photocurrent spectral responses of the devices were measured using a solar cell–photodetector responsivity measurement system (model DSR-100UV-B, Zolix), which was equipped with a lock-in amplifier (model SR-830, Standford Research Systems) for weak signal detection and with a 500 W quartz tungsten halogen lamp as the light

source. The incident light intensity was determined with a calibrated silicon photodetector for wavelengths between 400 and 900 nm and a calibrated InGaAs photodetector for wavelengths between 900 and 1,000 nm. A set of cutoff filters were used to remove unwanted higher-order wavelengths and other scattered light from the monochromator. Grazing incidence X-ray diffraction was performed at beamline 7.3.3 at the Lawrence Berkeley National Laboratory. The sample was placed inside a helium chamber and a Pilatus 2 M detector was used to collect the signal. RSoXS was performed at beamline 11.0.1.2 of the Lawrence Berkeley National Laboratory. Thin films were flowed and transferred onto a Si_3N_4 substrate and the experiment was carried out in transition mode using carbon K-edge photon energy. Dynamic secondary ion mass spectroscopy (DSIMS) measurements were performed with a 6650 Quadrupole SIMS system using O^+ ions as the primary ions. The beam diameter was 20 μm and the raster was 350 μm. Base pressure was kept below 1×10^{-9} torr.

Received 28 April 2014; accepted 7 January 2015; published online 9 February 2015

References

1. Li, G., Zhu, R. & Yang, Y. Polymer solar cells. *Nature Photon.* **6,** 153–161 (2012).
2. Li, Y. F. Molecular design of photovoltaic materials for polymer solar cells: toward suitable electronic energy levels and broad absorption. *Acc. Chem. Res.* **45,** 723–733 (2012).
3. You, J. *et al.* A polymer tandem solar cell with 10.6% power conversion efficiency. *Nature Commun.* **4,** 1446 (2013).
4. Blakesley, J. C. & Neher, D. Relationship between energetic disorder and open-circuit voltage in bulk heterojunction organic solar cells. *Phys. Rev. B* **84,** 075210 (2011).
5. Garcia-Belmonte, G. & Bisquert, J. Open-circuit voltage limit caused by recombination through tail states in bulk heterojunction polymer–fullerene solar cells. *Appl. Phys. Lett.* **96,** 113301 (2010).
6. Thakur, A. K., Wantz, G., Garcia-Belmonte, G., Bisquert, J. & Hirsch, L. Temperature dependence of open-circuit voltage and recombination processes in polymer–fullerene based solar cells. *Sol. Energy Mater. Sol. Cells* **95,** 2131–2135 (2011).
7. He, Z. C. *et al.* Enhanced power-conversion efficiency in polymer solar cells using an inverted device structure. *Nature Photon.* **6,** 591–595 (2012).
8. Liao, S. H., Jhuo, H. J., Cheng, Y. S. & Chen, S. A. Fullerene derivative-doped zinc oxide nanofilm as the cathode of inverted polymer solar cells with low-bandgap polymer (PTB7-Th) for high performance. *Adv. Mater.* **25,** 4766–4771 (2013).
9. Liu, Y. *et al.* Aggregation and morphology control enables multiple cases of high-efficiency polymer solar cells. *Nature Commun.* **5,** 6293 (2014).
10. Liang, Y. Y. *et al.* For the bright future—bulk heterojunction polymer solar cells with power conversion efficiency of 7.4%. *Adv. Mater.* **22,** E135–E138 (2010).
11. Li, W. W., Furlan, A., Hendriks, K. H., Wienk, M. M. & Janssen, R. A. Efficient tandem and triple-junction polymer solar cells. *J. Am. Soc. Chem.* **135,** 5529–5532 (2013).
12. Brabec, C. J. *et al.* Origin of the open circuit voltage of plastic solar cells. *Adv. Funct. Mater.* **11,** 374–380 (2001).
13. Blom, P. W. M., Mihailetchi, V. D., Koster, L. J. A. & Markov, D. E. Device physics of polymer:fullerene bulk heterojunction solar cells. *Adv. Mater.* **19,** 1551–1566 (2007).
14. Vandewal, K., Tvingstedt, K., Gadisa, A., Inganäs, O. & Manca, J. V. On the origin of the open-circuit voltage of polymer–fullerene solar cells. *Nature Mater.* **8,** 904–909 (2009).
15. Veldman, D. *et al.* Compositional and electric field dependence of the dissociation of charge transfer excitons in alternating polyfluorene copolymer/fullerene blends. *J. Am. Chem. Soc.* **130,** 7721–7735 (2008).
16. Zhang, M., Wang, H., Tian, H., Geng, Y. & Tang, C. W. Bulk heterojunction photovoltaic cells with low donor concentration. *Adv. Mater.* **23,** 4960–4964 (2011).
17. Yang, B. *et al.* Solution-processed fullerene-based organic Schottky junction devices for large-open-circuit-voltage organic solar cells. *Adv. Mater.* **25,** 572–577 (2013).
18. Cowan, S. R., Roy, A. & Heeger, A. J. Recombination in polymer–fullerene bulk heterojunction solar cells. *Phys. Rev. B* **82,** 245207 (2010).
19. Boix, P. P., Guerrero, A., Marchesi, L. F., Garcia-Belmonte, G. & Bisquert, J. Current–voltage characteristics of bulk heterojunction organic solar cells: connection between light and dark curves. *Adv. Energy Mater.* **1,** 1073–1078 (2011).
20. Maurano, A. *et al.* Recombination dynamics as a key determinant of open circuit voltage in organic bulk heterojunction solar cells: a comparison of four different donor polymers. *Adv. Mater.* **22,** 4987–4992 (2010).
21. Hawks, S. A. *et al.* Relating recombination, density of states, and device performance in an efficient polymer:fullerene organic solar cell blend. *Adv. Energy Mater.* **3,** 1201–1209 (2013).
22. Guerrero, A. *et al.* Charge carrier transport and contact selectivity limit the operation of PTB7-based organic solar cells of varying active layer thickness. *J. Mater. Chem. A* **1,** 12345–12354 (2013).
23. Guerrero, A. *et al.* How the charge-neutrality level of interface states controls energy level alignment in cathode contacts of organic bulk-heterojunction solar cells. *ACS Nano* **6,** 3453–3460 (2011).
24. Koster, L. J. A., Mihailetchi, V. D., Ramaker, R. & Blom, P. W. M. Light intensity dependence of open-circuit voltage of polymer:fullerene solar cells. *Appl. Phys. Lett.* **86,** 123509 (2005).
25. Garcia-Belmonte, G. *et al.* Influence of the intermediate density-of-states occupancy on open-circuit voltage of bulk heterojunction solar cells with different fullerene acceptors. *J. Phys. Chem. Lett.* **1,** 2566–2571 (2010).
26. Ripolles, T. S., Guerrero, A. & Garcia-Belmonte, G. Polymer defect states modulate open-circuit voltage in bulk-heterojunction solar cells. *Appl. Phys. Lett.* **103,** 243306 (2013).
27. Street, R. A. & Schoendorf, M. Interface state recombination in organic solar cells. *Phys. Rev. B* **81,** 205307 (2010).
28. Nayak, P. K., Garcia-Belmonte, G., Kahn, A., Bisquert, J. & Cahen, D. Photovoltaic efficiency limits and material disorder. *Energy Environ. Sci.* **5,** 6022–6039 (2012).
29. Liu, F. *et al.* Understanding the morphology of PTB7:PCBM blends in organic photovoltaics. *Adv. Energy Mater.* **4,** 1301377 (2014).
30. Ma, W. *et al.* Domain purity, miscibility, and molecular orientation at donor/acceptor interfaces in high performance organic solar cells: paths to further improvement. *Adv. Energy Mater.* **3,** 864–872 (2013).

Acknowledgements

The authors thank M. Yun and X. Wang for device performance verification. H.W., Z.H. and Y.C. thank the National Nature Science Foundation of China (nos. 51225301, 51403066, 91333206 and 51010003), the Fundamental Research Funds for the Central Universities (2014ZM001) and the Ministry of Science and Technology of China (2014CB643500) for financial support. F.L. and T.P.R. thank Polymer-Based Materials for Harvesting Solar Energy (PHaSE), an Energy Frontier Research Center funded by the US Department of Energy, Office of Basic Energy Sciences (DE-SC0001087), for support. The Advanced Light Source is supported by the Director, Office of Science, Office of Basic Energy Sciences, of the US Department of Energy under contract no. DE-AC02-05CH11231.

Author contributions

H.W., Z.H. and B.X. conceived the idea and designed the experiments. Z.H. fabricated and characterized the devices. F.L., C.W. and T.P.R. conducted structure characterizations. Y.Y. and S.X. synthesized the electron donor. H.W. and Y.C. coordinated and directed the study. All authors contributed to manuscript preparation, data analysis and interpretation, and discussed the results.

Additional information

Supplementary information is available in the online version of the paper. Reprints and permissions information is available online at www.nature.com/reprints. Correspondence and requests for materials should be addressed to H.W.

Competing financial interests

The authors declare no competing financial interests.